Supporting Information

Polysulfates block SARS-CoV-2 uptake via electrostatic interactions

Chuanxiong Nie,[a], [b] Paria Pouyan,[a] Daniel Lauster,[a] Jakob Trimpert,[b] Yannic Kerkhoff,[c] Gergo Peter Szekeres,[a], [d] Matthias Wallert,[c] Stephan Block,[c] Anil Kumar Sahoo,[e], [f] Jens Dernedde,[g] Kevin Pagel,[a], [d] Benedikt B. Kaufer,[b] Roland R. Netz,[e] Matthias Ballauff,[a] Rainer Haag[a]

---

[a] Institut für Chemie und Biochemie, Freie Universität Berlin, Arnimallee 22, 14195 Berlin, Germany
E-mail: chuanxnie@zedat.fu-berlin.de (C. Nie), Haag@zedat.fu-berlin.de (R. Haag)

[b] Institut für Virologie, Freie Universität Berlin, Robert-von-Ostertag-Str. 7-13, 14163 Berlin, Germany

[c] Department of Chemistry and Biochemistry, Emmy-Noether Group "Bionanointerfaces", Freie Universität Berlin, Arnimallee 22, 14195 Berlin, Germany

[d] Department of Molecular Physics, Fritz Haber Institute of the Max Planck Society, Faradayweg 4-6, 14195 Berlin, Germany
E-mail: gpszekeres@fhi-berlin.mpg.de (G. Szekeres)

[e] Fachbereich Physik, Freie Universität Berlin, Arnimallee 14, 14195 Berlin, Germany
E-mail: 201992kumarsahoo@gmail.com (A.K. Sahoo)

[f] Max Planck Institute of Colloids and Interfaces, Am Mühlenberg 1, 14476 Potsdam, Germany

[g] Institut für Laboratoriumsmedizin, Klinische Chemie und Pathobiochemie, Charité-Universitätsmedizin Berlin, Augustenburgerplatz. 1, 13353 Berlin, Germany

Experimental Procedures

Materials. Anhydrous solvents (dimethylformamide and toluene), benzoylated cellulose dialysis tubes (2000Da, 32 mm width) and heparin (sodium salt from porcine intestinal mucosa, H3393-500KU) were purchased from Merck (Darmstadt, Germany). Pentosan sulfate is obtained from Bene Arzneimittel GmbH, Munich, Germany. All other chemicals were bought from Merck (Darmstadt, Germany) unless stated otherwise.

Methods. Elemental composition determination was performed on a Vario EL CHNS element analyzer by Elementar Analysensysteme GmbH (Langselbold, Germany). ^{1}H NMR spectra were recorded on a Bruker AMX 500 (Bruker Corporation) or Jeol ECP 500 (JEOL GmbH). Chemical shifts (δ) are reported in ppm via the deuterated solvent peak as the standard. GPC measurements in water were performed with an Agilent 1100 equipped with an automatic injector, isopump, and Agilent 1100 differential refractometer (Agilent Technologies, Santa Clara,

1

CA, USA). The PSS Suprema (pre-column, 1x with pore size of 30 Å, 2x with pore size of 1000 Å (all of them with a particle size of 10 µm) column, was calibrated against Pullulan standards prior to measurements. The GPC measurements in THF were done with an Agilent Security (1200 Serie), equipped with automatic injector, isopump, and UV and RI detector. The separation was done via a PL gel from Agilent (1x pre-column, 3x Mixed-C with a particle size of 5 µm), which was calibrated against polystyrene standards. The GPC measurements in wate were performed on an Agilent 1100 from Agilent technologies equipped with isopump. The column was calibrated with pullulan standards prior to measurements,

Synthesis of linear polyglycerol sulfate (LPGS). Linear polyglycerol (LPG) was firstly synthesized by anionic ring opening polymerization of ethoxyethyl glycidyl ether,[1-2] followed by deprotection in slightly acidic media.

Synthesis of ethoxyethyl glycidyl ether (EEGE). The acetal protection of glycidol was done slightly modified to a reported protocol.[3] In summary, in an ice bath glycidol (70 mL, 1.052 mol, 1 eq.) of glycidol was mixed under stirring with divinyl ether (403.3 mL, 4.21 mol, 4 eq.) and p-TsOH.H_2O (2 g, 0.0105 mol, 0.01 eq.) was slowly added to the mixture. After 4 hours the reaction was quenched and washed with saturated $NaHCO_3$ solution. The organic phase was dried over sodium sulfate and concentrated under reduced pressure. The crude product was dried over CaH_2 and distilled under vacuum over preheated molecular sieve and stored under argon in freezer until further use. Due to storage under dry and inert conditions, weighing of the final product was not possible and complete conversion of starting material is assumed.

^{1}H NMR (500 MHz, ACETONE-D_6) δ 4.70 (qd, J = 5.3, 2.4 Hz, 1H), 3.77 (dd, J = 11.5, 3.0 Hz, 1H), 3.73 – 3.57 (m, 1H), 3.50 – 3.41 (m, 1H), 3.30 (dd, J = 11.5, 6.4 Hz, 1H), 3.12 – 3.00 (m, 1H), 2.69 (ddd, J = 5.3, 4.1, 2.1 Hz, 1H), 2.52 (ddd, J = 11.9, 5.2, 2.6 Hz, 1H), 1.22 (t, J = 5.3 Hz, 3H), 1.12 (td, J = 7.1, 1.1 Hz, 3H).

Polymerization of ethoxyethyl glycidyl ether (PEEGE) and deprotection to LPG. The polymerization was done based on a reported protocol. (Macromolecules 2010, 43 (4), 1778-1784.) In summary for 20 kDa LPG: In a flame-dried Schlenck flask Oct$_4$NBr (172.78 mg, 0.310 mmol, 0.0047 eq.) was dried under high vacuum and dissolved in 60 mL dry toluene. Afterwards EEGE (10 mL, 65.6 mmol, 1 eq.) was added under inert conditions. Then in an ice bath i-Bu$_3$Al (1.4 mL, 1.55 mmol, 0.023 eq.) was added all at once. The reaction was let to proceed overnight, thereafter quenched by addition of 1 mL of EtOH. The excess of activator was precipitated in cold Et$_2$O. The product was dialyzed in acetone (MWCO: 2kDa) for further purification. After

drying, the product was obtained as 8.38 g colorless viscous oil (50%). (GPC THF- $\overline{M_n}$: 32.4 kDa, PDI: 1.07). ^{1}H NMR (500 MHz, ACETONE-D6) δ 4.81 – 4.60 (m, 1H), 3.83 – 3.32 (m, 7H, monomer unit), 1.33 – 1.22 (m, 3H), 1.14 (t, 3H). The acetal groups were then deprotected in a solution of 3% HCl (37%) in EtOH. The mixture was stirred overnight and then purified by dialysis against water (MWCO:2 kDa). (GPC water- $\overline{M_n}$: 17.7 kDa, PDI: 1.2).

Synthesis of hyperbranched polyglycerols. Hyperbranched polyglycerol (hPG) was synthesized by ring-opening multibranching polymerization of glycidol in a heterogenous reaction mixture in dioxane. This method only allowed the molecular weight of hPG to be increased to only 800-900 kDa. To obtain the high-molecular weight hPG, a two-step polymerization is used as reported in our previous studies.[4]

First, a macroinitiator was synthesized in a heterogenous reaction mixture in dioxane. Dry trimethylolpropane (120 mg, 0.89 mmol, 1.0 eq.) was partially deprotonated (30 % OH) with potassium methoxide (67 µL, 0.27 mmol, 0.3 eq., 25 % in methanol) in argon atmosphere at 60 °C for 30 min. After the addition of 24 mL dioxane (dry) the turbid mixture was heated to 100 °C. Glycidol (12 mL, 0.18 mol, 201 eq.) was slowly added (0.5 ml h^{-1}) via syringe pump into the reaction mixture. The polymer was purified by removing the dioxane, precipitation as methanolic solution in acetone and dialysis against water in regenerated cellulose membrane (10 kDa MWCO). The resulted hPG was obtained with a yield of 93.6 %.

In the second step, this hPG was used as macroinitiator to grow the polymer further. 2.5 g (0.034 mol, total OH groups) of the lyophilized polymer was dissolved in dry DMF (35 mL). The polymer was partially deprotonated with the addition of potassium hydride in oil (30 wt.%) (80 µg, 272 µL, 2.0 µmol). The temperature was increased to 100 °C and glycidol (25 mL, 0.37 mol) were added with a rate of 0.9 mL h^{-1}. After precipitation in acetone and dialysis against water in regenerated cellulose membrane (50 kDa MWCO) the resulted molecular weight was 2.6 MDa with a Đ of 1.4.

Sulfation of the polyglycerols. All the polymers were sulfated according to an already published protocol with slight adjustments[5] The completely dry corresponding polymer was dissolved in dry DMF (10 mL for 1 g). The mixture was then heated up to 60 °C and respective amount of SO$_3$/pyridine (1.5 eq. of -OH groups) was added. The mixture was let stir overnight under inert atmosphere. Thereafter the pH was brought to 13 by addition of 1M NaOH to the solution. Then the polymer was dialyzed against saturated solution of NaCl for 2 days and 2

days in water. After drying in high vacuum, the crude product was obtained as white solid powder. The degree of functionalization was determined via elemental analysis.

Plaque reduction assay. SARS-CoV-2 München (SARS-CoV2M; BetaCoV/Germany/BavPat1/2020) was propagated on Vero E6 cells and titrated via plaque assay.[6] For a plaque reduction assay, Vero E6 cells were grown in a 12-well plate. The virions (approx. 100PFU) were firstly incubated with the compound at different concentrations for 1 hour, prior to the incubation with Vero E6 cells for 1 hour. The cells were washed with PBS once and then cultured in Avicel overlay medium for 2 days. After being fixed by the addition of 4% formaldehyde, the cells were stained with 0.75% crystal violet (aqueous solution) to count plaques. The experiment was performed in BSL3 laboratory at the Institut für Virologie, Freie Universität Berlin. The plaque reduction ratio was calculated by comparing treated samples with the non-treated virus controls as follows:

$$Plaque\ reduction\ (\%) = (1 - \frac{Plaque\ number\ (sample)}{Plaque\ number\ (virus\ control)}) \times 100\%$$

The IC50 value was estimated by '[inhibitor] vs. response' model in GraphPad Prism 7.0.

Virus binding to Vero E6 cells. The virions were inactivated by 4% formaldehyde for 24 hours in BSL3 under appropriate biosafety conditions. The formaldehyde inactivated SARS-CoV-2 virions were purified and concentrated by ultracentrifugation (100, 000 rpm, 2h) with 20% sucrose solution. The pellet was resuspended in PBS and stored at -80 °C before usage.

To study virus attachment, the virions were firstly labelled with 3,3′-Dioctadecyl-oxacarbocyanin-perchlorate (DiO, ThermoFisher Scientific, USA). For the labelling, 100 µL virus solution was incubated with 5 µL 20 µM DiO (ethanol) for 45 min. Then, the free dye was removed by spinning column (Protein A HP SpinTrap™, GE Healthcare, Germany). For the inhibitor binding, 10 µL labelled virions was incubated with 90 µL inhibitor solution (1000 µg/mL) for 45 min at 37 °C. The mixture was incubated with Vero E6 cells for 1 h on ice. The unbound virus was removed by washing with PBS. The cell nucleus was stained with DAPI, and then the cells were visualized by confocal laser scanning microscopy (SP8, Leica, Germany).

Image analysis for virus binding. Quantification of bound virus particles per cell was performed by a self-written ImageJ macro. The nuclei were segmented from the background using a machine learning classifier of the Trainable Weka Segmentation plugin of ImageJ. The output probability maps of the nuclei were blurred with a Gaussian filter (radius = 5) and the

touching nuclei were segmented by thresholding the background and finding local maxima (Process > Find Maxima... > Output type: Segmented Particles). The automatically detected nuclei were then manually checked and recounted and corrected if necessary. Images showing the virus particles were scaled up by a factor of 3 using bicubic interpolation to decrease pixel noise. Quantification was also performed by thresholding the background and finding local maxima which correspond to the virus particles. Virus particles per cell were determined for 4 images per sample which were then used to calculate mean and standard deviation. Paired t-tests were used to find statistically significant differences between samples.

Mass spectrometry experiments. 1 mg/mL RBD (Thermofisher, Germany), 14.6 mg/mL LPGS, and 7.6 mg/mL heparin solutions were purified by filtering through an Amicon® Ultra 3 kDa molecular weight cut-off filter (Merck, Germany) twice, which also facilitated the buffer exchange into 250 mM pH 7 ammonium acetate solution. After their purification, the LPGS and heparin solutions were diluted five-fold, and 0.4 µL, 0.8 µL, and 1.2 µL of them were mixed respectively with 4.0 µL RBD solution. The samples were loaded into Pd/Pt-coated nano-ESI capillaries produced in-house and introduced in positive ion mode at a capillary voltage of 1000 V into a Synapt G2 S instrument modified with a linear drift tube ion mobility cell. The spectra were recorded in TOF-only mode to provide softer conditions for the formed complexes in the gas phase. At least two data sets were acquired for each sample, and spectra were collected with 1 s acquisition time for 5-20 min depending on the signal intensity.

Due to the natural heterogeneity of the LPGS and heparin samples, background-correction was necessary for both the RBD-LPGS and the RBD-heparin data sets. For background correction, the spectra of the pure LPGS and heparin were acquired, mean-smoothed, and normalized for an m/z position where the pure RBD spectrum exhibits low signal intensity, while the pure LPGS or heparin spectrum exhibit high signal intensities; then, the as-normalized LPGS or heparin spectrum was subtracted from the corresponding mean-smoothed RBD-LPGS or RBD-heparin spectra.

Microscale thermophoresis. Experiments were conducted with a Monolith NT.115 (NanoTemper) from the laboratory of Prof. Heberle (FU Berlin). For the measurements His-tagged RBD of the SARS-CoV-2 S-protein from recombinant expression in mammalian cells was kindly provided by Dr. Coskun (TU Dresden). For the experiments, twofold dilution series of human ACE2 (novoprotein, kindly provided by Prof. Bader at MDC Berlin), LPGS, HPGS and heparin were mixed with a final concentration of 50 nM NHS-Red (NanoTemper) labeled RBD.

Protein labeling and purification was performed with a 2nd generation NHS-Red labeling kit. The labeling efficiency was analyzed from spectroscopic measurements (Nanodrop) to be approximately 1:1 (protein:dye). The measurements were performed in DPBS and premium capillaries (NanoTemper) at 25°C, and default settings for the measurement runs (Initial fluorescence=5s, thermophoresis=30s, and recovery=5s). Obtained data were analyzed with a gating strategy 1.5 s after the start of the infrared laser, and data were fitted as previously shown.[7]

MD simulations. The coordinates for the wild type RBD of the SARS-CoV-2 spike protein were obtained from the deposited crystal structure (PDB ID: 6M0J). Two different RBD mutants (E484K or N501Y mutations) were built using PyMOL. The structure of the heparin pentamer was built using CHARMM-GUI *Glycan Reader & Modeler.*[8] The structure of LPGS undecamer was built using Avogadro software.[9] CHARMM36m[10] and CHARMM Carbohydrates[11][12] force field parameters were used to model the protein and Heparin, respectively. Parameters and partial atomic charges for LPGS were obtained using the CGenFF program[13],[14] and CHARMM General force field.[15][16] CHARMM-compatible TIP3P water[17][18] and ion parameters[19] were used. RBD/LPGS and RBD/Heparin were arranged and solvated in boxes of sizes $7\times7\times9.5$ nm^3 and $7\times7\times10$ nm^3, as shown in Figure 5a,b (manuscript), respectively. Enough Na$^+$ ions were added to charge neutralize each system, then Na$^+$ / Cl$^-$ ion pairs were added to obtain a 150 mM NaCl solution estimated from the mole fraction of ion pairs and water. The simulation for each case was performed at least for 500 ns in the *NpT* ensemble at *T* = 300 K and *p* = 1 bar with *periodic boundary condition* in *xyz* directions, using GROMACS 2020.1 package.[20] The stochastic velocity rescaling thermostat[21] with a time constant of τ_T = 0.1 ps was used to control the temperature, while for the pressure control an isotropic Parrinello-Rahman barostat[22] was used with a time constant of τ_p = 2 ps and a compressibility of κ = 4.5×10^{-5} bar^{-1}. The LINCS algorithm[23] was used to constrain the bonds involving H-atoms, allowing a timestep of Δt = 2 fs. Electrostatics interactions were computed using the particle mesh Ewald (PME) method[24] with a real-space cutoff distance of 1.2 nm, while van der Waals (VDW) interactions were modeled using Lennard-Jones potentials with a cutoff distance of 1.2 nm where the resulting forces smoothly switch to zero between of 1 nm to 1.2 nm.

Simulation data analysis. The electrostatic potential map of the protein was calculated using the APBS tool[25] and visualized using VMD.[26] Simulation snapshots were rendered using VMD as well.

Number of close contacts: A contact is defined by an atom of LPGS/Heparin falling within 3 Å of any atom of the protein residue. The total number of contacts averaged over the last 100 ns of simulation data is presented in the main text.

Persistence length: The persistence length *P* of a polymer can be estimated from the polymer's Kuhn length *b*, using the well-known relationship for the *worm like chain* model: $P = b/2$. The Kuhn length, *b*, is related to the contour length L_0 and the end-to-end distance *R* of a polymer via the expression: $b = \langle R^2 \rangle / L_0$, where $\langle \cdot \rangle$ represents the time average. So, the persistence length was calculated using $P = \langle R^2 \rangle / 2L_0$, where $\langle R^2 \rangle$ and L_0 were obtained from 200 ns of simulation data where the polymer is not attached to the protein. L_0, *R,* and *P* for both LPGS and Heparin are given in the inset of Figure 5d in the main text.

Cell viability. The cells, including A549 cells, Vero E6 cells and human bronchial epithelial cell (HBE), were seeded in a 96-well plate at a density of 1×10^4 cells/well in DMEM medium. After 24 hours, the compounds were added to each well at a final concentration of 0.1 µg/mL to 1 mg/mL. The cells were cultured for another 24 hours with compounds dispersed in the medium. Finally, the viabilities of the cells were investigated with a CCK-8 assay according to the manuals, for which the result was revealed by optical absorbance at 450 nm. Cell without any compounds was set as positive control, while 1% SDS solution was set as the negative control. The biocompatibility of the compounds was studied by comparing with the positive and negative controls as shown follows:

$$Cell\ viability\ (\%) = (\frac{ABS450\ (compounds) - ABS450\ (negativle\ control)}{ABS450(positive\ control)}) \times 100\%$$

Activated partial thromboplastin time (aPTT). The anticoagulating activity for the samples was revealed by activated partial thromboplastin time of the plasma treated with the samples.[27] Briefly, 100 µL plasma (Siemens Healthcare, Erlangen, Germany) and 100 µL Actin FS (Siemens Healthcare, Erlangen, Germany) were mixed and incubated (3 min, 37 °C) with 4 µL samples in different concentrations. H_2O was set as the control. The reaction was started by the addition of 100 µL of prewarmed (37 °C) clotting activator $CaCl_2$.
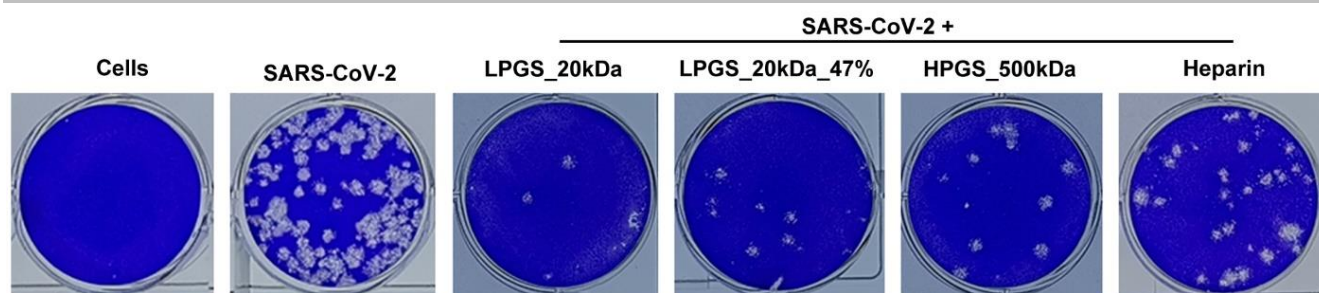
Results and Discussion

Figure S1. Plaque images for SARS-CoV-2 treated with different compounds at 50µg/mL.
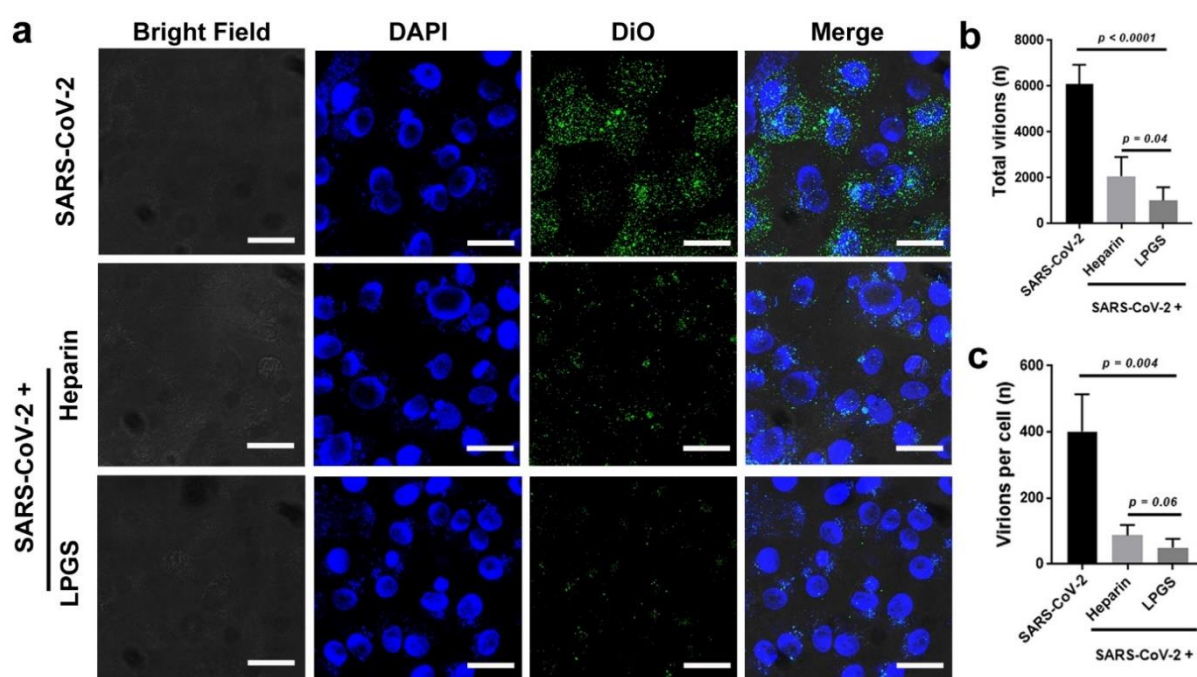

Figure S2. (a) CLSM image for the virus binding to Vero E6 cells in presence of the compounds. Scale bar: 10 µm. (b, c) Analysis of virus binding to Vero E6 cells from CLSM images for the number of virions. Values are expressed as mean ±SD, n=4. The addition of concentrated heparin (1 mg/mL) can also reduce the binding of SARS-CoV-2, probably because of steric shielding of virions by heparin at high dose.
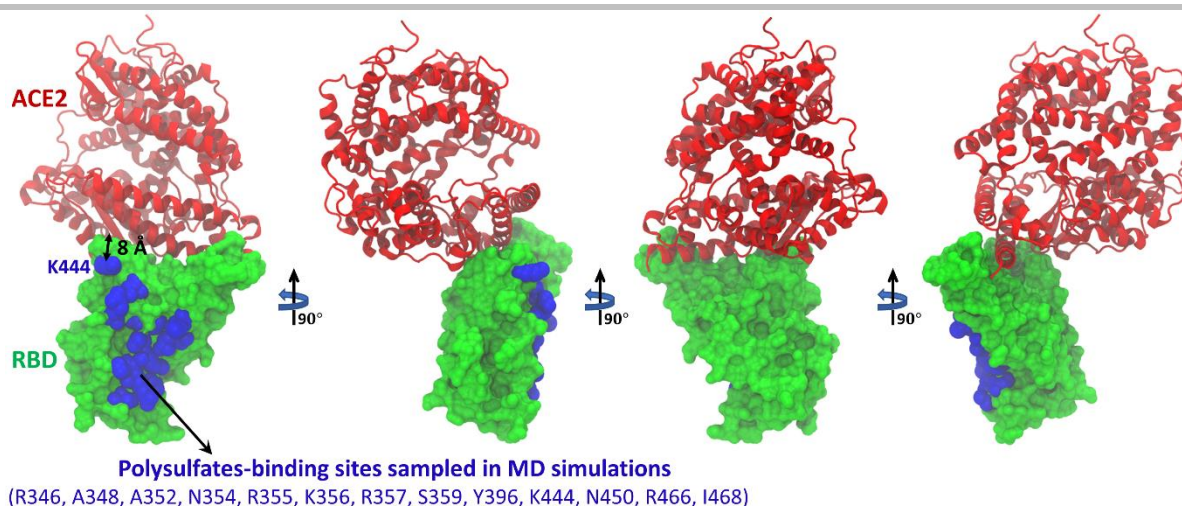
Polysulfates-binding sites sampled in MD simulations
(R346, A348, A352, N354, R355, K356, R357, S359, Y396, K444, N450, R466, I468)

Figure S3. Distribution of HS binding site on the RBD of SARS-CoV-2. ACE2 is shown in secondary structure representation (red), whereas RBD is shown in surface representation (green). The amino acid residues of RBD (R346, A348, A352, N354, R355, K356, R357, S359, Y396, K444, N450, R466, I468) found to form contacts with the polysulfates in MD simulations are highlighted in VDW representation (blue), denoting the putative HS-binding site.
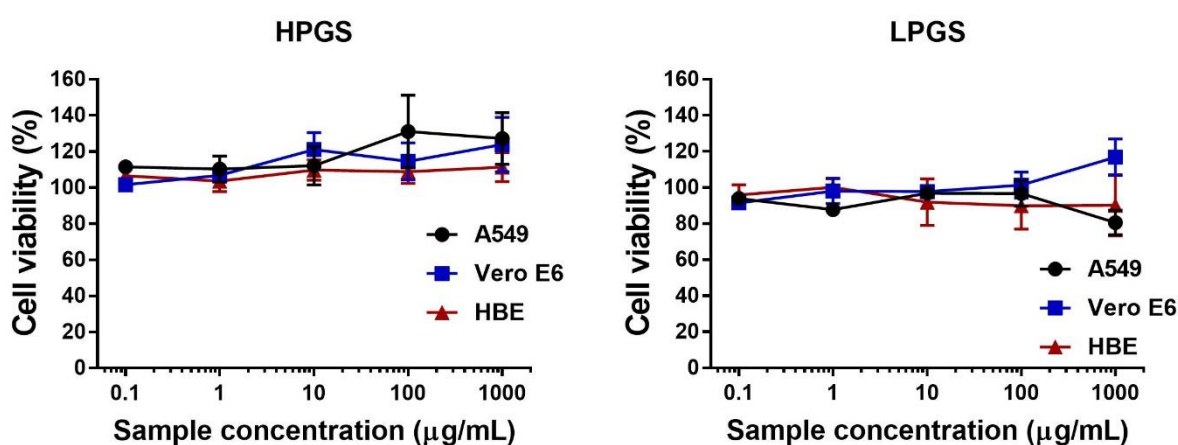

Figure S4. Evaluation of cellular toxicity of polyglycerol sulfates, against A549, Vero E6 and HBE cells, respectively. Values are expressed as mean ±SD, n=3.
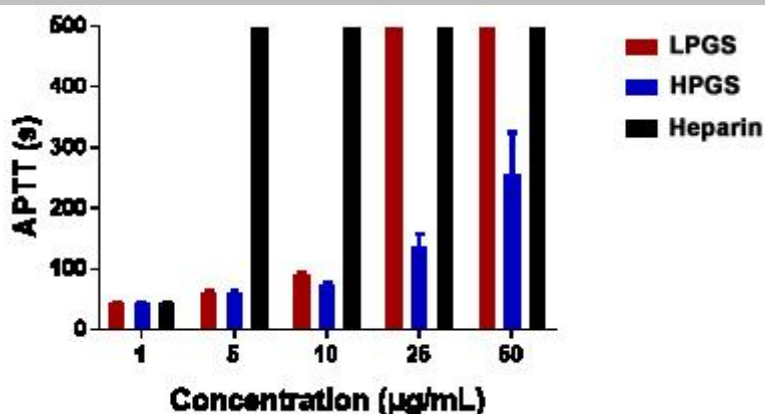
Figure S5. Activated partial thromboplastin time (aPTT) of plasma treated with polysulfates at different concentrations. Values are expressed as mean ±SD, n=3.

References

[1]   M. Weinhart, I. Grunwald, M. Wyszogrodzka, L. Gaetjen, A. Hartwig, R. Haag, *Chem. Asian J.* **2010**, *5*, 1992-2000.
[2]   M. Weinhart, D. Gröger, S. Enders, S. B. Riese, J. Dernedde, R. K. Kainthan, D. E. Brooks, R. Haag, *Macromol. Biosci.* **2011**, *11*, 1088-1098.
[3]   M. Gervais, A.-L. Brocas, G. Cendejas, A. Deffieux, S. Carlotti, *Macromolecules* **2010**, *43*, 1778-1784.
[4]   M. Wallert, C. Nie, P. Anilkumar, S. Abbina, S. Bhatia, K. Ludwig, J. N. Kizhakkedathu, R. Haag, S. Block, *Small* **2020**, *16*, 2004635.
[5]   H. Türk, R. Haag, S. Alban, *Bioconjug. Chem.* **2004**, *15*, 162-167.
[6]   R. Wölfel, V. M. Corman, W. Guggemos, M. Seilmaier, S. Zange, M. A. Müller, D. Niemeyer, T. C. Jones, P. Vollmar, C. Rothe, M. Hoelscher, T. Bleicker, S. Brünink, J. Schneider, R. Ehmann, K. Zwirglmaier, C. Drosten, C. Wendtner, *Nature* **2020**, *581*, 465-469.
[7]   S. Bhatia, D. Lauster, M. Bardua, K. Ludwig, S. Angioletti-Uberti, N. Popp, U. Hoffmann, F. Paulus, M. Budt, M. Stadtmüller, T. Wolff, A. Hamann, C. Böttcher, A. Herrmann, R. Haag, *Biomaterials* **2017**, *138*, 22-34.
[8]   S.-J. Park, J. Lee, Y. Qi, N. R. Kern, H. S. Lee, S. Jo, I. Joung, K. Joo, J. Lee, W. Im, *Glycobiology* **2019**, *29*, 320-331.
[9]   M. D. Hanwell, D. E. Curtis, D. C. Lonie, T. Vandermeersch, E. Zurek, G. R. Hutchison, *J. Cheminformatics* **2012**, *4*, 17.
[10]   J. Huang, S. Rauscher, G. Nawrocki, T. Ran, M. Feig, B. L. de Groot, H. Grubmüller, A. D. MacKerell, *Nat. Methods* **2017**, *14*, 71-73.
[11]   O. Guvench, S. S. Mallajosyula, E. P. Raman, E. Hatcher, K. Vanommeslaeghe, T. J. Foster, F. W. Jamison, A. D. MacKerell, *J. Chem. Theory Comput.* **2011**, *7*, 3162-3180.
[12]   S. S. Mallajosyula, O. Guvench, E. Hatcher, A. D. MacKerell, *J. Chem. Theory Comput.* **2012**, *8*, 759-776.
[13]   K. Vanommeslaeghe, A. D. MacKerell, *J. Chem. Inf. Model.* **2012**, *52*, 3144-3154.
[14]   K. Vanommeslaeghe, E. P. Raman, A. D. MacKerell, *J. Chem. Inf. Model.* **2012**, *52*, 3155-3168.
[15]   K. Vanommeslaeghe, E. Hatcher, C. Acharya, S. Kundu, S. Zhong, J. Shim, E. Darian, O. Guvench, P. Lopes, I. Vorobyov, A. D. Mackerell Jr., *J. Comput. Chem.* **2010**, *31*, 671-690.
[16]   W. Yu, X. He, K. Vanommeslaeghe, A. D. MacKerell Jr., *J. Comput. Chem.* **2012**, *33*, 2451-2468.
[17]   W. L. Jorgensen, J. Chandrasekhar, J. D. Madura, R. W. Impey, M. L. Klein, *J. Chem. Phys.* **1983**, *79*, 926-935.
[18]   A. D. MacKerell Jr, D. Bashford, M. Bellott, R. L. Dunbrack Jr, J. D. Evanseck, M. J. Field, S. Fischer, J. Gao, H. Guo, S. Ha, *J. Phys. Chem. B* **1998**, *102*, 3586-3616.
[19]   R. M. Venable, Y. Luo, K. Gawrisch, B. Roux, R. W. Pastor, *J. Phys. Chem. B* **2013**, *117*, 10183-10192.
[20]   M. J. Abraham, T. Murtola, R. Schulz, S. Páll, J. C. Smith, B. Hess, E. Lindahl, *SoftwareX* **2015**, *1-2*, 19-25.
[21]   G. Bussi, D. Donadio, M. Parrinello, *J. Chem. Phys.* **2007**, *126*, 014101.
[22]   M. Parrinello, A. Rahman, *J. Appl. Phys.* **1981**, *52*, 7182-7190.
[23]   B. Hess, *J. Chem. Theory Comput.* **2008**, *4*, 116-122.

[24]   T. Darden, D. York, L. Pedersen, *J. Chem. Phys.* **1993**, *98*, 10089-10092.
[25]   N. A. Baker, D. Sept, S. Joseph, M. J. Holst, J. A. McCammon, *Proc. Natl. Acad. Sci.* **2001**, *98*, 10037-10041.
[26]   W. Humphrey, A. Dalke, K. Schulten, *J. Mol. Graph. Model.* **1996**, *14*, 33-38.
[27]   S. Reimann, D. Gröger, C. Kühne, S. B. Riese, J. Dernedde, R. Haag, *Adv. Healthc. Mater.* **2015**, *4*, 2154-2162.